Ultrafast vibrational energy redistribution within C–H and O–H stretching modes of liquid methanol

ARTICLE *in* CHEMICAL PHYSICS LETTERS · MAY 2000

Impact Factor: 1.9 · DOI: 10.1016/S0009-2614(00)00356-0

2 AUTHORS:

Lawrence Iwaki
University of Illinois, Urbana-Champai…
15 PUBLICATIONS **795** CITATIONS
SEE PROFILE

Dana D Dlott
University of Illinois, Urbana-Champai…
297 PUBLICATIONS **6,631** CITATIONS
SEE PROFILE

5 May 2000

ELSEVIER

Chemical Physics Letters 321 (2000) 419–425

CHEMICAL PHYSICS LETTERS

www.elsevier.nl/locate/cplett

Ultrafast vibrational energy redistribution within C–H and O–H stretching modes of liquid methanol

Lawrence K. Iwaki [1], Dana D. Dlott *

School of Chemical Sciences, University of Illinois at Urbana-Champaign, Box 01-6 CLSL, 600 S. Goodwin Ave., Urbana, IL 61801, USA

Received 17 December 1999; in final form 24 February 2000

Abstract

An ultrafast IR–Raman technique is used to study fast redistribution of vibrational energy within CH and OH stretching vibrations of liquid methanol. The instantaneous population distribution throughout the entire CH and OH stretch region ($2700–3700\ cm^{-1}$) is probed simultaneously. The fast redistribution produces a nonthermal population distribution within CH and OH stretching excitations. The nonequilibrium CH stretch population occurs because different CH stretching modes have different lifetimes. The nonequilibrium OH stretch population occurs when OH stretching excitations that are pumped by the laser on the red edge of the band undergo spectral diffusion toward the band center.

1. Introduction

In this Letter, we use the IR–Raman technique [1,2] to investigate vibrational energy redistribution within C–H and O–H stretching vibrations of liquid methanol. With recent improvements in laser technology [3], our signal-to-noise ratio has become good enough to examine this interesting process with unprecedented detail. In the IR–Raman method, a tunable mid-infrared (mid-IR) pulse selectively pumps a vibrational transition, and a time-delayed visible pulse monitors subsequent population dynamics including vibrational energy relaxation (VER) and spectral diffusion via incoherent anti-Stokes Raman scattering [1,2,4,5].

In the earliest IR–Raman experiments [1,6], when a C–H stretching transition was pumped in the mid-IR, an instantaneous rise of C–H stretch excitation was observed in other C–H stretching transitions predominant in the Raman spectrum, leading to the idea of energy redistribution among C–H stretching vibrations [6–13] that is faster than VER out of the C–H stretch states. Fast redistribution certainly simplifies the interpretation of IR–Raman experiments, since then it does not matter which C–H transition is pumped or probed. Fendt et al. [8] developed a theoretical model for the rapid redistribution and applied it to a number of liquids. Over the years, this problem has been revisited many times [2], most recently in studies of ethanol monomers in CCl_4 [7,12–14].

There are some noteworthy experimental and theoretical difficulties with previous works in this area. It is desirable to monitor in real time both the disappearance of the pumped C–H stretching transi-

* Corresponding author. E-mail: dlott@scs.uiuc.edu

[1] Present address: National Institute of Standards and Technology, Gaithersburg, MD, USA.

0009-2614/00/$ - see front matter
PII: S0009-2614(00)00356-0

tion and the appearance of excitation in other C–H stretch or C–H bending first overtone transitions coupled by Fermi resonance [8–10]. That has not been accomplished until the present work. In addition, previous experiments have not accurately accounted for artifacts that hinder the observation of the initial state at short times. In IR–Raman, artifacts are created by sum-frequency generation (SFG) [15,16]. As mentioned in Ref. [8], much data prior to 1981 was contaminated by SFG artifacts. It is not correct that using perpendicular polarizations will eliminate these effects, as stated in Ref. [8], because they can arise from quadrupolar coupling to the radiation field [15,16].

Previous models of the fast redistribution process, for states with separations $\geqslant kT$, used the following expression for the lifetime of the initial state [8,10,17],

$$T_1 = R^{-1}\left[\exp(\omega/\Omega)\right]^{2/3} T_2(f), \qquad (1)$$

where R is an anharmonic coupling matrix element, $\hbar\omega$ is the energy gap between the states, Ω is a characteristic solvent frequency (typically 100–200 cm^{-1}) and $T_2(f)$ is the time constant for vibrational dephasing of the final state. Eq. (1) gives the initial rate of leaving the pumped state. In Ref. [8] it was claimed that vibrational energy 'equilibrates' among nearby states when the rate of redistribution among these states is much faster than the rate for energy loss (VER) from these states. Knowing only the leaving rate, it is impossible to say what an equilibrium distribution might be. In quantum mechanics where microscopic reversibility holds, $k_{i\to f} = k_{f\to i}$, suggesting that equilibrium involves a uniform distribution, with the same amount of excitation in every state. On the other hand, at sufficiently long time thermal equilibrium must be attained.

We have chosen to study methanol, rather than ethanol which has been studied extensively in this context [6–8,13,18]. In ethanol, the VER lifetime is rather long ($T_1 = 12$ ps) which has been attributed to a relatively poor mismatch between the frequencies of the C–H stretching and C–H bending first overtone transitions [8]. However in ethanol, redistribution among C–H stretching transitions is very fast (< 0.5 ps), and it is complicated by the possibility of energy transfer among the methyl and methylene stretching vibrations [13]. In methanol, which has been much less studied, a much shorter T_1 [8] has been attributed to a better frequency match between the C–H stretching and C–H bending first overtones [8]. Absent is the complication of having two carbon atoms and two types of C–H stretching vibrations.

IR and Raman spectra of methanol are shown in Fig. 1, labeled with assignments from Ref. [19]. In methanol the relevant states are symmetric ν_s(CH) and antisymmetric ν_a(CH) stretching vibrations of the methyl group, symmetric δ_s(CH) and antisymmetric δ_a(CH) bending vibrations, and ν(OH) [20]. The broad linewidth of the ν(OH) transition is due to the simultaneous coexistence of a wide range of hydrogen-bonding environments [21,22]. C–H stretching transitions were pumped with mid-IR pulses at 2870 or 3033 cm^{-1}, as indicated in Fig. 1a. The pump bandwidth (indicated by the little curves in Fig. 1) of ~ 35 cm^{-1} was narrow enough to produce selective excitation of either ν_s(CH) or ν_a(CH).

In our methanol experiments, we acquired data simultaneously over the entire ~ 1000 cm^{-1} wide spectral range of CH and OH stretching transitions. It then becomes possible to characterize and eliminate effects of SFG coherence artifacts. A theoretical model is used to interpret the data, based on a fully quantum mechanical treatment of the bath dynamics [23].

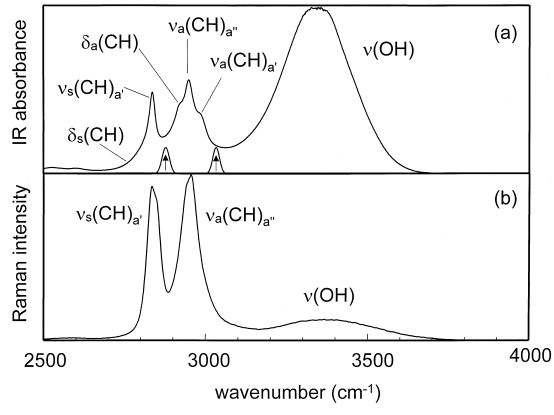

Fig. 1. IR and Raman spectrum of neat methanol (point group C_s), with assignments from Ref. [19]. The arrows indicate the center wavelengths of the pump pulses. δ(CH) refers to the first overtone of CH bending vibrations.

2. Experimental

The IR–Raman system, consisting of a ~ 1 ps Ti:Sapphire laser and a two-color optical parametric amplifier, has been discussed previously [3,16]. The pump pulses (3.47 or 3.30 μm, 50 μJ, ~ 0.8 ps, 35 cm^{-1} FWHM, 200 μm diameter) and probe pulses (0.532 μm, 5 μJ, ~ 0.8 ps, 25 cm^{-1} FWHM, 150 μm diameter) were focused on a flowing jet of reagent grade methanol (Aldrich), and anti-Stokes emission was detected by a multichannel spectrograph. The likelihood of pumping C–H stretch overtones is at most a few percent, since the incident pump fluence of ~ 0.15 J/cm^2 is about one-tenth of the saturation fluence of ~ 1.5 J/cm^2 and the overtone transition is redshifted by ~ 20 cm^{-1} from the pump pulse, assuming the redshift is about the same as in ethanol [13].

In IR–Raman experiments with mid-IR pump ω_{IR} and visible Raman probe ω_L, an SFG artifact can appear near $t = 0$ at the anti-Stokes shift $\omega_L + \omega_{IR}$ that is the same location in the anti-Stokes spectrum where the pumped transition is observed. Although SFG is forbidden in bulk liquids in the dipole approximation [24], quadrupole and other higher-order terms of the multipole expansion can lead to SFG signals that can compete with the weak IR–Raman signal [16]. The time and frequency dependence of the SFG artifact can be characterized by replacing the sample with a thin (50 μm) KTP crystal [16].

A computer program was used to fit the transient anti-Stokes spectra to a sum of Voigt lineshapes plus a Gaussian to represent the coherence artifact, as shown in Fig. 2. The computed Gaussian was subtracted from the spectrum, to yield the displayed data in Figs. 3 and 4, and the Voigt intensities were used to determine the time-dependence in the first panel of each figure. The ν_a(CH) and ν_s(CH) transitions

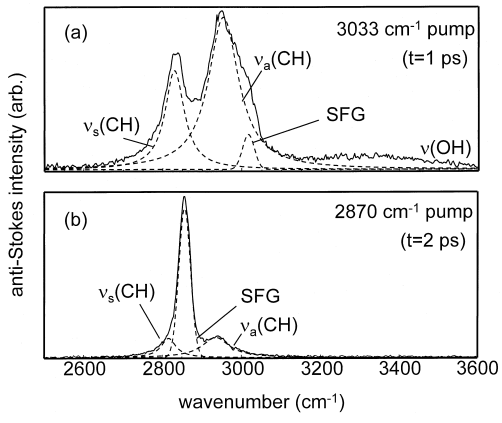

Fig. 2. Two representative transient anti-Stokes spectra, showing how the SFG artifact is removed. The spectra are fitted by a computer to a pair of Voigt lineshapes to represent ν_a(CH) and ν_s(CH), and a Gaussian to represent the artifact.

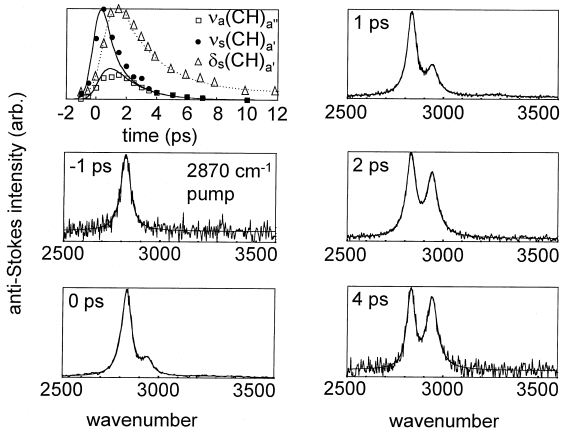

Fig. 3. Methanol data with 2870 cm^{-1} pump. Top left: time dependence of ν_a(CH), ν_s(CH) and δ_s(CH) intensities (symbols). The solid curves are fits to Eqs. (7). Other panels: normalized spectra with SFG artifact subtracted.

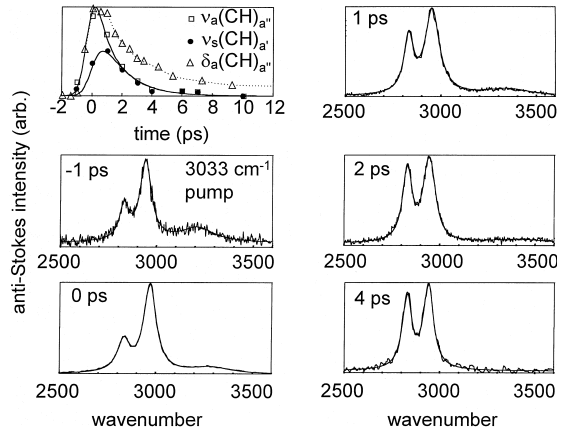

Fig. 4. Methanol data with 3033 cm^{-1} pump. Top left: time dependence of ν_a(CH), ν_s(CH) and δ_a(CH) intensities (symbols). The solid curves are fits to Eqs. (7). Other panels: normalized spectra with SFG artifact subtracted.

were pumped somewhat off peak, as indicated in Fig. 1, to help distinguish the artifact from the C–H stretching transition. The bending vibration δ_a(CH) and δ_s(CH) intensities were determined by fitting the spectrum [25] with Voigt lineshapes centered at 1466 and 1531 cm^{-1}.

3. Results

Fig. 3 shows methanol data with 2870 cm^{-1} pumping of ν_s(CH). The first panel shows the time dependent intensities of the ν_s(CH), ν_a(CH) and δ_s(CH) states; the other panels show spectra normalized to the same height. The ν_s(CH) intensity rises instantaneously and the ν_a(CH) and_δ_s(CH) intensities follow more slowly. The time dependences indicate that ν_a(CH) and δ_s(CH) populations are generated by ν_s(CH) decay. At longer times (e.g., 4 ps) the intensity ratio ν_s(CH)/ν_a(CH) is about 1.1:1.

Fig. 4 shows methanol data with 3033 cm^{-1} pumping of ν_a(CH). The ν_a(CH) signal rises instantaneously, and the ν_s(CH) signal follows more slowly. The δ_a(CH) signal also rises instantaneously. In a subsequent publication [25], we will show that the δ_a(CH) signal we see at short times is due to the overtone $v = 2 \rightarrow 1$ transition, indicating that the δ_a(CH) first overtone is directly pumped by the laser [16,26,27]. The δ_a(CH) overtone acquires IR absorption strength via Fermi resonance with the ν_a(CH) fundamental [8]. At longer times the intensity ratio ν_s(CH)/ν_a(CH) is about 1:1.1. A new feature not seen in Fig. 3 is significant ν(OH) population. At early times (i.e., -1 ps in Fig. 4), the peak of the ν(OH) population is at ~ 3210 cm^{-1}. As time increases, the population shifts to the blue. The peak is at 3280 cm^{-1} at 0 ps and 3360 cm^{-1} at 1 ps. The ν(OH) lifetime is somewhat shorter than the ν(CH) lifetime. After a few picoseconds all ν(OH) has vanished and only ν(CH) remains.

As a point of reference, we simulated the anti-Stokes spectrum for two limiting cases: (1) a uniform distribution, with every CH and OH stretch having the same (unit) population; and (2) a thermal equilibrium distribution at 295 K. The Stokes Raman spectrum $I_{St}(\nu)$ is represented as [1,4]

$$I_{St}(\nu) = \text{const}[1 + n_\nu(T)]\,\sigma(\nu)(\nu_L - \nu)^4, \qquad (2)$$

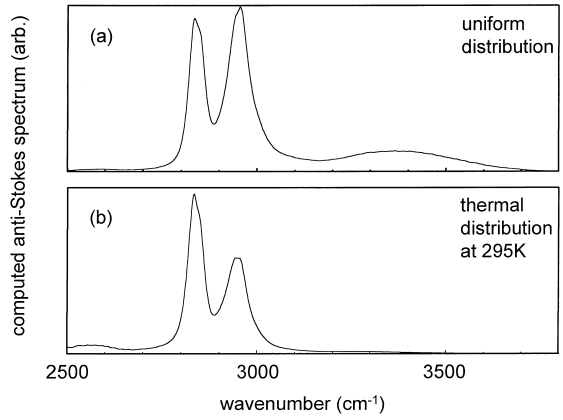

Fig. 5. Computed anti-Stokes spectra of methanol for a 'uniform' distribution where every CH and OH stretch is equally populated, and for a thermal distribution at 295 K.

where the constant depends on the apparatus, $n_\nu(T) = [1 - \exp(-h\nu/kT)]^{-1}$ is the thermal occupation number, $\sigma(\nu)$ is the Raman cross-section, and ν_L is the laser frequency. The anti-Stokes spectrum for a uniform distribution is

$$I_{St}(\nu) = \text{const}[1]\sigma(\nu)(\nu_L + \nu)^4. \qquad (3)$$

For vibrations in the 3000–3600 cm^{-1} range, $n_\nu(T) \ll 1$, so by measuring the Stokes spectrum of methanol (Fig. 1b) and multiplying it by $(\nu_L + \nu)^4/(\nu_L - \nu)^4$, we obtain Eq. (3), plotted in Fig. 5a. For a thermal distribution, we multiply Eq. (3) by $n_\nu(T)$, as shown in Fig. 5b. Using Fig. 5 as a guide, nothing even close to a thermal distribution is ever seen in Figs. 3 and 4. After a few picoseconds, we see roughly equal ν_s(CH) and ν_a(CH) intensities close to a uniform distribution. However we see far too much ν(OH) in Fig. 4 for either a uniform or a thermal distribution.

4. Discussion

The rate constant for VER of state σ, a vibration of frequency Ω of a polyatomic liquid (the 'system'), is given by [23]

$$K_\sigma = (\hbar)^{-2}\int_{-\infty}^{+\infty}\langle V_R(t)V_R\rangle \times\left(\sum_{\sigma'}|\langle\sigma|V_S|\sigma'\rangle|^2 e^{it\Omega_{\sigma\sigma'}}\right)dt, \qquad (4)$$

where σ' labels final states, V_R is the reservoir Hamiltonian that includes other intramolecular vibrations and lower energy collective vibrations of the liquid ('phonons' [23]), and V_S is the system Hamiltonian. Eq. (4) shows the decay rate is proportional to the sum of the Fourier components of fluctuating forces exerted by the reservoir at frequencies $\Omega_{\sigma\sigma'}$ [23,28,29]. For polyatomic molecules, V_S is usually expanded in normal coordinates to describe VER via cubic, quartic or higher-order anharmonic couplings [23,30]. CH stretch VER in methanol involves exciting CH bending (~ 1500 cm^{-1}) and CO bending (~ 1350 cm^{-1}) daughter vibrations [25] plus phonons. Quartic or higher-order anharmonic couplings are needed to describe CH stretch decay, since three or more daughter excitations are produced for every CH stretch.

Fig. 1 shows the ν_a(CH) and ν_s(CH) vibrations are separated by ~ 120 cm^{-1}. Therefore with the relatively narrow-band mid-IR pump pulses used here, energy transfer between these vibrations cannot occur without the absorption or emission of at least one phonon. The lowest order process involves cubic anharmonic coupling and a single phonon. The rate constant for ν_a(CH) $\rightarrow$ ν_s(CH) via cubic anharmonic coupling is [30],

$$k_{a\rightarrow s} = 36\pi^2 \sum_{\omega_{ph}} \langle V^{(3)}\mathrm{s,a},\omega_{ph}\rangle^2 \times \left(n_{\omega_{ph}}(T)+1\right)\delta(\omega_a-\omega_s-\omega_{ph}). \quad (5)$$

The fluctuating forces on ω_a are produced by the lower energy intramolecular vibration ω_s and a phonon ω_{ph}. In Eq. (5), $V^{(3)}$ is the cubic anharmonic matrix element coupling ν_a(CH), ν_s(CH), and a phonon with $\omega_{ph} = \hbar(\omega_a - \omega_s)$. Eq. (5) describes two down-conversion processes, temperature independent spontaneous phonon emission and temperature dependent stimulated emission. The rate constant for energy transfer from the lower energy ν_s(CH) to the higher energy ν_a(CH) state is [30],

$$k_{s\rightarrow a} = 36\pi^2 \sum_{\omega_{ph}} \langle V^{(3)}\mathrm{s,a},\omega_{ph}\rangle^2 n_{\omega_{ph}}(T)\,\delta \times(\omega_a-\omega_s-\omega_{ph}). \quad (6)$$

Eq. (6) describes a temperature dependent up-conversion process involving one-phonon absorption. Eqs. (5) and (6) satisfy detailed balance. The ratio of up to down rate constants $k_{s\rightarrow a}/k_{a\rightarrow s} = \exp(-\hbar(\omega_a - \omega_s)/kT)$.

The fast redistribution can be treated by a master equation,

$$\frac{d\nu_s}{dt} = -(k_s + k_{s\rightarrow a})\nu_s + k_{a\rightarrow s}\nu_a + \frac{I(t)\alpha_s}{h\nu_s}, \quad (7a)$$

and

$$\frac{d\nu_a}{dt} = k_{s\rightarrow a}\nu_s - (k_a + k_{a\rightarrow s})\nu_a, \quad (7b)$$

where k_s and k_a are rate constants for VER. Equations 7 are correct when the mid-IR pulse, with intensity $I(t)$, pumps the ν_s(CH) transition with absorption cross-section α_s. When the laser pumps the ν_a(CH) transition, the pumping term should be moved to Eq. (7b) and the cross-section α_a and energy $h\nu_a$ should be used. Equations 7 were evaluated numerically by approximating the apparatus response function as a Gaussian with a 1 ps FWHM [3], and were fit to the data in the first panels of Figs. 3 and 4. The ratio $k_{s\rightarrow a}/k_{a\rightarrow s}$, must be $\exp(-120\ \mathrm{cm}^{-1}/kT) \approx 0.56$, leaving three parameters k_s, k_a and $k_{a\rightarrow s}$ to be varied.

Because $k_{a\rightarrow s} > k_{s\rightarrow a}$, if the two VER rate constants k_a and k_s were equal, the intensities would eventually go to the $\sim 2{:}1$ ν_s(CH):ν_a(CH) ratio in Fig. 5b for thermal equilibrium. Since the observed intensity ratio is actually closer to 1:1, ν_s(CH) must decay somewhat faster than ν_a(CH). The best fit was obtained with a 1 ps ν_s(CH) lifetime, a 5 ps ν_a(CH) lifetime, and a time constant $(k_{a\rightarrow s})^{-1}$ of 1.6 ps. The smooth curves in the first panels of Figs. 3 and 4 show that the data are fit very well with this choice of parameters. The fit worsened noticeably when the parameters were varied by more than 25% from these values. The only relevant data for methanol in the literature is a single measurement on methanol monomers in CCl_4. Fendt et al. [8] pumped and probed the ν_a(CH) state, and observed an initial decay with a 1.5 ps time constant, that was interpreted as the ν_a(CH) lifetime. Those data agree with our work but the interpretation does not. The ν_a(CH) lifetime is actually 5 ps. The initial decay out of ν_a(CH) is determined by the 1.6 ps time constant for energy transfer to ν_s(CH).

In theoretical models often used to describe ν(CH) decay in molecular liquids (Refs. [8,10] and references therein), the ν(CH) lifetime is ordinarily determined by the strength of Fermi resonance between the stretch and the bend overtone. The reverse appears to be true in methanol. The longer-lived ν_a(CH) ($T_1 = 5$ ps) has a strong Fermi resonance with the δ_a(CH) bend overtone [8], as indicated by the IR spectrum in Fig. 1 and the simultaneous pumping of the stretch and bend overtone seen in Fig. 4. The shorter-lived ν_s(CH) ($T_1 = 1$ ps) has a weaker Fermi resonance with the δ_s(CH) overtone as indicated by the low IR absorbance associated with the δ_s(CH) overtone in Fig. 1 and the delayed rise of δ_s(CH) in Fig. 3. These observations indicate that near resonance with CH bending overtones does not always determine the CH stretch VER rate. In the case of methanol, the rapid decay of ν_s(CH) is due not to coupling to the first overtone of δ_s(CH), but rather to combination bands of δ(CH) and δ(OH) [25].

The OH stretching results in Fig. 4 are explained by a quite different mechanism. There is little energy transfer between OH and CH stretching excitations in methanol [25]. Most ν(OH) excitation occurs because mid-IR pulses at 3033 cm^{-1} pump the red edge of the ν(OH) transition (see Fig. 1a). Fig. 4 shows that excitations produced near the red edge undergoes picosecond time scale spectral diffusion toward the center of the transition, as observed previously in studies of ν(OH) spectral diffusion of water [15] and HDO in D_2O [31]. There is a well-known correlation between the location in the ν(OH) band and the strength of hydrogen bonding [21,22]. The red edge corresponds to the strongest hydrogen bonding. The spectral diffusion indicates a change in the local environment toward average or weak hydrogen bonding. That may occur by an evolving local structure or by energy migration [12,13,15,32]. With 3033 cm^{-1} pumping, in just 1 or 2 ps, ν(OH) excitations are observed at 3400 cm^{-1} — a highly nonthermal distribution close to the uniform distribution shown in Fig. 5a. The energy required to generate excitations at 3400 cm^{-1} with 3033 cm^{-1} pumping comes from breaking strong hydrogen bonds and reforming weaker hydrogen bonds [33]. The nearly uniform distribution of excitation in the ν(OH) region occurs because the energy of configurations with higher ν(OH) frequencies and weaker hydrogen bonding is about the same as configurations with lower ν(OH) frequency and stronger hydrogen bonding.

5. Conclusion

The fast vibrational redistribution process after methanol CH excitation has been measured by simultaneously monitoring the excited state population distribution at all frequencies in the CH and OH stretching region. After fast redistribution, the CH population distribution is far from a thermal distribution because the lifetimes of ν_s(CH) and ν_a(CH) modes differ by a factor of five. The OH stretching excitations, which are incidentally excited at the red edge when ν_a(CH) is pumped, undergo spectral diffusion toward the center of the transition, producing higher energy ν_{OH} excitations that also are far from thermal equilibrium with the CH stretch excitations.

Acknowledgements

We thank John C. Deàk for his many contributions. This material is based on work supported by the National Science Foundation under award number DMR-9714843, and by the Air Force Office of Scientific Research under contract F49620-97-1-0056. L.K.I. acknowledges support from an AASERT fellowship, DAAG55-98-1-0191, from the Army Research Office.

References

[1] A. Laubereau, W. Kaiser, Rev. Mod. Phys. 50 (1978) 607.
[2] A. Seilmeier, W. Kaiser, in: W. Kaiser (Ed.), Ultrashort Laser Pulses and Applications, Vol. 60, Springer Verlag, Berlin, 1988, p. 279.
[3] J.C. Deàk, L.K. Iwaki, D.D. Dlott, Opt. Lett. 22 (1997) 1796.
[4] M. Hofmann, H. Graener, Chem. Phys. 206 (1995) 129.
[5] M. Hofmann, R. Zürl, H. Graener, J. Chem. Phys. 105 (1996) 6141.
[6] K. Spanner, A. Laubereau, W. Kaiser, Chem. Phys. Lett. 44 (1976) 88.
[7] R. Laenen, C. Rauscher, Chem. Phys. Lett. 274 (1997) 63.
[8] A. Fendt, S.F. Fischer, W. Kaiser, Chem. Phys. 57 (1981) 55.
[9] W. Zinth, C. Kolmeder, B. Benna, A. Irgens-Defregger, S.F. Fischer, W. Kaiser, J. Chem. Phys. 78 (1983) 3916.

[10] H. Graener, A. Laubereau, Appl. Phys. B. 29 (1982) 213.
[11] H. Graener, A. Laubereau, Chem. Phys. Lett. 133 (1987) 378.
[12] R. Laenen, C. Rauscher, A. Laubereau, J. Phys. Chem. A 101 (1997) 3201.
[13] R. Laenen, C. Rauscher, A. Laubereau, Chem. Phys. Lett. 283 (1998) 7.
[14] R. Laenen, K. Simeonidis, Chem. Phys. Lett. 299 (1999) 589.
[15] J.C. Deàk, L.K. Iwaki, D.D. Dlott, J. Phys. Chem., 2000, in press.
[16] J.C. Deàk, L.K. Iwaki, S.T. Rhea, D.D. Dlott, J. Raman Spectrosc. 2000, in press.
[17] W. Zinth, H.-J. Polland, A. Laubereau, W. Kaiser, Appl. Phys. B 26 (1981) 77.
[18] A. Laubereau, G. Kehl, W. Kaiser, Opt. Commun. 11 (1974) 74.
[19] T. Shimanouchi, Tables of Molecular Vibrational Frequencies: Consolidated Volume 1, US Dept. of Commerce, National Bureau of Standards, Washington, DC, 1972.
[20] G. Herzberg, Molecular Spectra and Molecular Structure II. Infrared and Raman Spectra of Polyatomic Molecules, Van Nostrand Reinhold, New York, 1945.
[21] U. Liddel, E.D. Becker, Spectrochim. Acta 10 (1957) 70.
[22] M. Matsumoto, K.E. Gubbins, J. Chem. Phys. 93 (1990) 1981.
[23] V.M. Kenkre, A. Tokmakoff, M.D. Fayer, J. Chem. Phys. 101 (1994) 10618.
[24] Y.R. Shen, Surf. Sci. 299/300 (1994) 551.
[25] L.K. Iwaki, D.D. Dlott, 2000, unpublished.
[26] J.C. Deàk, L.K. Iwaki, D.D. Dlott, J. Phys. Chem. 102 (1998) 8193.
[27] J.C. Deàk, L.K. Iwaki, D.D. Dlott, J. Phys. Chem. A, 1998, in press.
[28] D.W. Oxtoby, in: J. Jortner, R.D. Levine, S.A. Rice (Eds.), Photoselective Chemistry, Part 2, Vol. 47, Wiley, New York, 1981, p. 487.
[29] S.A. Egorov, K.F. Everitt, J.L. Skinner, J. Phys. Chem. A. 103 (1999) 9494.
[30] S. Califano, V. Schettino, N. Neto, Lattice Dynamics of Molecular Crystals, Springer-Verlag, Berlin, 1981.
[31] G.M. Gale, G. Gallot, F. Hache, N. Lascoux, S. Bratos, J.-C. Leicknam, Phys. Rev. Lett. 82 (1999) 1068.
[32] S. Woutersen, H.J. Bakker, Nature 402 (1999) 507.
[33] A. Luzar, D. Chandler, Nature 379 (1996) 55.